J Mater Sci: Mater Med (2008) 19:1051–1060
DOI 10.1007/s10856-007-3197-0

The influence of residual stress on the shear strength between the bone and plasma-sprayed hydroxyapatite coating

Yung-Chin Yang · Chyun-Yu Yang

Received: 12 June 2006 / Accepted: 23 May 2007 / Published online: 15 August 2007

Abstract Plasma-sprayed HA coating (HAC) 50 and 200 μm thick on Ti6Al4V cylinders was transcortically implanted in the femora of canines. Push-out testing of implant-bone interfaces showed that the HAC coating exhibited higher shear strength at 50 μm coating than 200 μm one. The plasma-sprayed HACs were exhibited compressive residual stresses and the thicker HAC exhibited higher residual stress than that of the thinner HAC. Due to the structure for 50 and 200 μm implants were the same, meaning similar cohesive strength of the lamellar splats. And, there was no difference in the physiological environment; hence the difference of the shear strength for the 50 and 200 μm-HAC implants could best be attributed to the compressive residual stress existed in the HA coating.

Introduction

The industrial use of plasma-sprayed coating is sometimes limited by the stresses generated during deposition [1]. Different stress states occur during the various stages of the deposition process. During the initial contact of the sprayed molten materials with the substrate, a quenching stress, always tensile, is induced within the coating [2, 3]. During the cooling stage, a thermal stress gradient appears in the through-section of the coating/substrate system. Residual stress in the coating might vary with the coating thickness [4, 5], spraying parameter and substrate temperature [3, 6]. More importantly, the residual stress could deteriorate the HAC with or without the immersion in simulated body fluid [6, 7].

Sergo et al. [8] suggested that residual stress might exert a major effect in the long-term chemical stability of the hydroxapatite coatings. The compressive residual stress tended to heal the "mud cracking" of the typical plasma-sprayed HA coatings. It was inferred from their thermodynamic derivation that compressive load acting on the hydroxapatite could suppress the [OH^-] ions dissolved from the material. On the other hand, residual stress in the compressive state of plasma-sprayed ceramic coating on metal substrate was established to induce the through-thickness tensile stress in the system [6]. Figure 1 shows the effect of residual stress on the debonding of the coating where before debonding, an interface and inter-lamellar-splat crack was assumed to exist (Fig. 1a). In-plane residual stress would induce through-thickness tensile stress (σ_n, Fig 1b) acting in the direction normal to the interface of the HA coating and the Ti-substrate. This normal tensile stress would weak the adhesive strength of HAC to substrate.

The previous in vivo tests have demonstrated that [9–11], under the shear loading condition, the implants could fail at bone near the HAC–bone interface, at HAC–bone interface, between lamellar splats in the plasma-sprayed hydroxyapatite coating, and at HAC–Ti alloy substrate interface. The residual stress was reasonably suspected to act adversely on the lamellar splats in the plasma-sprayed hydroxyapatite coating, and at HAC–Ti alloy substrate interface. Nevertheless, the nature and magnitude of stress state and in vivo response of the stress in orthopaedic implants were rarely rigorously studied.

Y.-C. Yang (✉)
Department of Materials and Mineral Resources Engineering, Institute of Materials Science and Engineering, National Taipei University of Technology, Taipei, 106, Taiwan ROC
e-mail: ycyang@ntut.edu.tw

C.-Y. Yang
Department of Orthopaedics, National Cheng Kung University Medical Center, Tainan, Taiwan ROC

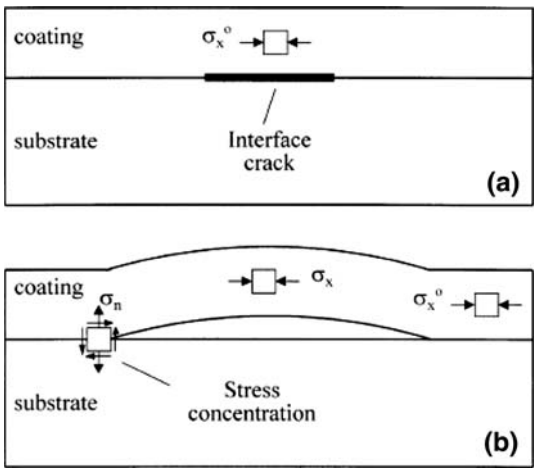

Fig. 1 Effect of delamination on coating fracture driving force: (**a**) non delaminated configuration, and (**b**) delaminated configuration

In the present study, we investigated the influence of coating thickness and its residual stress on the shear strength as well as the failure mode of plasma-sprayed HAC to bone. Plasma-sprayed HA-coated cylindrical Ti–6Al–4V rods were transcortically implanted in the femora of dogs. After 4, 6, 8, and 12 weeks, the implant-bone interfacial shear strength was measured by means of a push-out test. The failure mode at implant-bone interface was analyzed by scanning electron microscopy (SEM). The biaxial residual stress states of plasma-sprayed HACs on Ti–6Al–4V substrate were studied by using the "$sin^2\psi$" technique of the X-ray diffraction (XRD) method [12].

Materials and methods

Materials

Two implants with different coating thickness were evaluated: Ti–6Al–4V alloy with an HAC of 50 and 200 μm thicknesses. For the in vivo test, all implants were cylindrical in design and measured approximately 4.76 mm in diameter by 12 mm in length. The alloy substrates were slightly undersize by machining to accommodate the 200 μm or 50 μm thick layer of HA coating. For the residual stress measurement, the 22 mm (l) × 17 mm (w) × 3.3 mm (t) substrates of Ti–6Al–4V alloy was used. Commercial high purity feedstock HA powder (Amdry 6020, Sulzer Plasma Technik, Inc., Troy, MI 48084) was used in the coating process. Prior to spraying, the substrate surfaces were degreased to remove organic contaminants and blast with Al_2O_3 grits to effect the surface roughness. The HA coating was applied by means of an atmospheric plasma spray technique (APS, Plasma-Technik, M 1100-C, Sulzer Plasma Technik, Inc., Troy, MI 48084).

In vitro test of plasma-sprayed HACs

The SBF used was a modified protein-free Hank's balanced salt solution (HBSS) with ionic concentration close to that of human blood plasma (Table 1) [7]. Following an ultrasonic rinse in distilled water, the HA-coated specimens were cleaned using an ultrasonic wash in acetone and then put into the culture vials. Prior to soaking, the culture vials and specimens were sterilized by dry heat (120 °C, 8 h). Under the sterile environment, the SBF of 30 ml/cm^2 of HAC was added to the vials. The SBF was buffered at a pH of 7.2 with 50 mM tris–hydroxymethyl-aminomethane and 45 mM HCl [13]. The vials were then placed in a humidified, 5% CO_2/balance air incubator to minimize the change in initial pH; all immersions took place at 37 °C without stirring. After 1, 2, 3, and 4 weeks of immersion, the specimens were removed, washed in distilled water, and dried in the oven. Then, the cross-sectional micrographs of the coating were taken for quantitative analyses of the porosity content by using a computer image analyzer (OPTIMAS 6.0). The phase constituents of the immersed HACs and the as-sprayed HAC were identified by X-ray diffractometry (XRD). Moreover, the index of crystallinity (IOC%) of the HACs was evaluated from the ratio of the main peak intensities of the HAC (I_c) and the HA powder (I_p) by the relation of IOC (%) = (I_c/I_p) × 100%.

For measurement of Young's modulus in the HACs, the 1.0 mm-thick coating was coated on the Ti substrate of dimension 40 mm (l) × 10 mm (w) × 0.7 mm (t). The coating was separated from the Ti substrate by carefully grinding the latter from the back of the specimen, leaving the free HA coating as described in reference No. 12. Measurement of Young's modulus of HACs was carried out using a standard three-point bending test (ASTM E-855 [14]) by

$$E = \frac{PL^3}{4bh^3\delta}$$

where E is the Young's modulus, P is the load, L is the span length between supports, b is the specimen width, h is the specimen thickness, and δ is the deflection at midspan. Each measured value of Young's modulus represents an average of three tests.

The bonding strength of HACs was tested using a standard adhesion test (ASTM C-633) [15] that was especially designed for the plasma-sprayed coatings. For each immersion period, five specimens were tested.

Surgical technique

All implants were cleaned with ultrasonic wash in reagent grade acetone followed by ultrasonic rinse in distilled

Table 1 Electrolyte ion concentration of protein-free modified Hank's balanced salt solution (HBSS)

Species	NaCl	KCl	$CaCl_2$	KH_2PO_4	$NaHCO_3$
mg/l	8,000	400	140	60	350
Species	$MgCl_2 \cdot 6H_2O$	$Na_2HPO_4 \cdot 2H_2O$	$MgS0_4 \cdot 7H_2O$	Glucose	
mg/l	100	60	100	1,000	

water. Dry heat (120 °C, 8 h) sterilization was used prior to implantation. The lateral cortices of mongrel dogs weighing 10–15 kg were drilled transcortically by three-stage-hand reaming to the final diameter, using sterile surgical techniques (Fig. 2a). During all drilling procedures copious saline was used to minimize any bone thermal trauma and to remove the bone debris. Then, the cylindrical implants were inserted into pre-drilled holes by finger pressure (Fig. 2). A total of 120 implants were inserted into the femora of 12 dogs. Each dog contained five implants of 200 μm and five implants of 50 μm HA-coated Ti–6Al–4V (Fig. 2b).

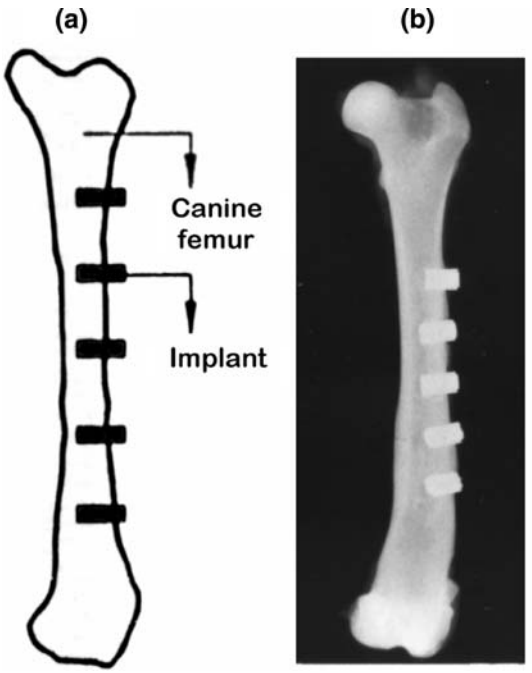

Fig. 2 (**a**) Schematic representation of the transcortical implantation model; (**b**) Specimen roentgenogram, obtained 12 weeks post-implantaion, of five HA-coated implants in canine femur

Mechanical testing

After 4, 6, 8, and 12 weeks, the dogs (three dogs at each period) were sacrificed. The intact femora were retrieved and cleared of soft tissue. By using a diamond saw, each implant site was isolated transversely and then bisected through the medullary cavity perpendicularly to the long axis of implant. As shown in Fig. 3, a trephine-type reamer made by 316 stainless steel was used to prepare a smooth endosteal bone surface surrounding each implant. Well-prepared, fresh specimens were placed in a testing jig, and the implants were pushed out from the surrounding bone using an Instron test machine (Fig. 3c). A loading rate of 0.2 mm/min was used for all tests. The force needed to loosen the implant was determined from the load to displacement curve. The shear strength of the interface was calculated by dividing the maximum push-out force by the total bone area in contact with the implant. This area was represented in the following formula: Area = πDH, where D is the diameter of the implant and H is the average cortex thickness (Fig. 3). After the push-out test, the disrupt implants were fixed in 10% buffered formalin solution, dehydrated in graduate ethyl alcohol solutions from 70 to 100%, and then carbon coated. The fractographs of implants were investigated by SEM (JEOL JSMr 840) for failure mode analysis.

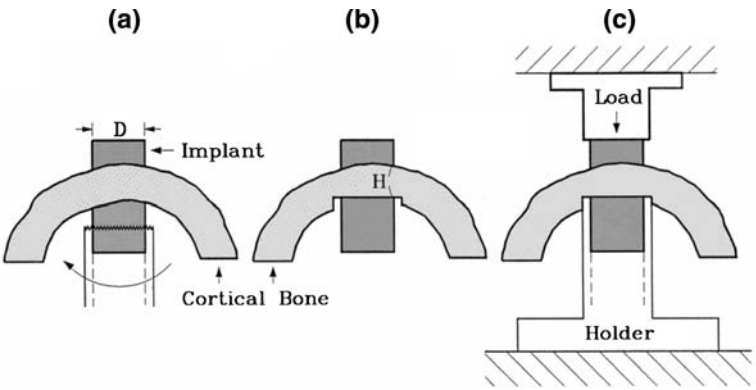

Fig. 3 Schematic representation of the push-out test for measuring the shear strength at the HAC–cortical bone interface. (**a**) Use the stainless steel holder with saw tooth to grind the inner cortical bone; (**b**) Prepared specimen; (**c**) Push the implant out under the Instron test machine. (D, diameter of implant; H, average thickness of cortical bone)

Residual stress measurement

Consider a portion of the surface of a stressed body (Fig. 4). ψ is the angle of tilt to the surface normal of the specimen. Diffraction measurements were taken at six ψ values (ψ = 0, 12.92, 18.43, 26.56, 30 and 33.21°), corresponding to 0.05 increments in $sin^2\psi$. The reflection (6 2 1) of hexagonal $Ca_{10}(PO_4)_6(OH)_2$ at approximately 2θ = 87.32° shown in Fig. 5 was used as the diffraction plane for lattice plane spacing measurement in the residual stress analysis, and the reflection of (5 3 2) of HA was employed for the calibration of 2θ angles. As detailed elsewhere by X-ray diffractometry, the residual stresses formed in HACs parallel to the spraying direction (σ_x) can be calculated as: [12]

$$\sigma_x = \frac{(d_i - d_n)/d_n}{\sin^2\psi} \cdot \frac{E}{(1+v)} \quad (2)$$

where ψ is the angle of tilt for the specimen, d_n is the crystallographic plane spacing measured at ψ = 0°, and d_i is the plane spacing measured in different ψ angles by XRD, v is the Poisson's ratio being 0.28, E is the Young's modulus. The residual stress (σ_x) can be obtained from the above equation by measuring the slope of $(d_i - d_n)/d_n/sin^2\psi$, which was determined from a least square fit of the plot of $(d_i - d_n)/d_n$ against $sin^2\psi$ ($\Delta d/d$ vs. $sin^2\psi$).

Results

In vitro characteristics of HACs

The diffractograms of HA powder (HAP), 50 μm-HAC, 200 μm-HAC and inner 200 μm-HAC are shown in Fig. 6. The major peak matches well with the standard HA phase

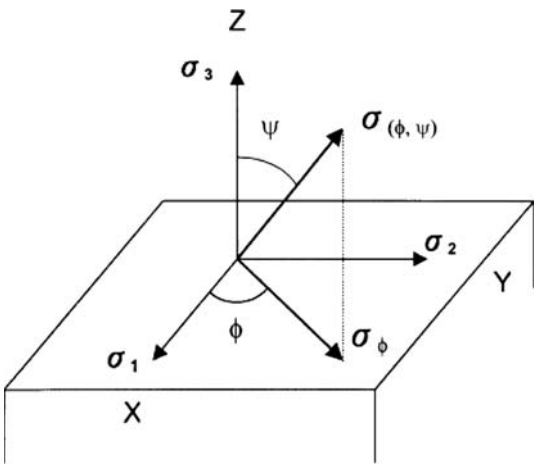

Fig. 4 Stresses at the surface of a stressed body where $\sigma_3 = 0$. The stress to be measured is σ_ψ

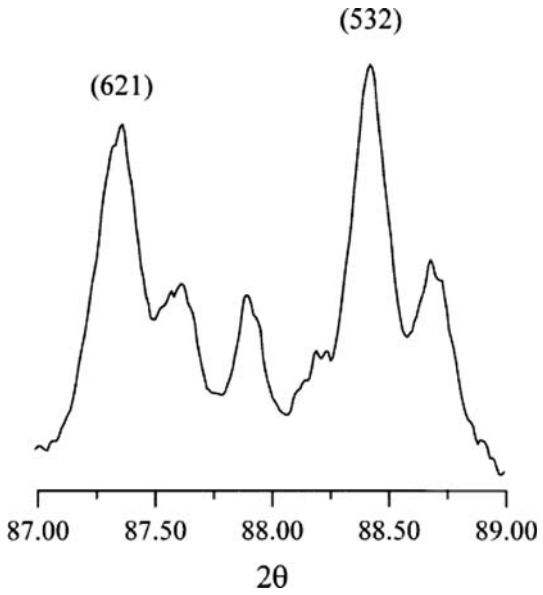

Fig. 5 X-ray diffractogram of as-received HAC powder in which the (6 2 1) reflecting plane was used for residual stress measurements

($Ca_{10}(PO_4)_6(OH)_2$, JCPDS No. 9-432). In addition, the HAP does not show any line-broadening effect and could serve as the standard of 100% crystallinity. Apart from the HA phase, several impurity phases including α-TCP ($Ca_3(PO_4)_2$), β-TCP, TP ($Ca_4P_2O_9$), and CaO were identified in the HACs. Moreover, it is noted that the crystallinity of the two sprayed HACs (50 and 200 μm) were decreased in contrast to that of the HAP. As listed in Table 2, the crystallinity of the 50 μm-HAC (IOC = 45.5%) revealed the similar one with the 200 μm-HAC (IOC = 47.8%). Moreover, as shown in Table 2, the crystallinity of the HACs increases significantly following the immersion in SBF. This finding is consistent with the results by de Groot et al. and Yang et al. [7, 16]. The increase of crystallinity is considered to generate not only from the dissolution of amorphous phase but also the crystallization of HA from the SBF [17]. The porosity content of the HACs after immersion were quantitatively analyzed from the cross-sectional SEM micrographs, and the result is shown in Table 2, which indicate that the porosity content varies from 5.2 to 9.1% of the two thickness HACs after 4 weeks of immersion.

Young's modulus of HACs

The Young's moduli of the 1 mm thick HACs obtained from the three-point bending test for the as-sprayed and the immersed HACs are shown in Table 2. The Young's modulus of 24.8 GPa assumes a maximum for the as-sprayed HAC. Following the immersion in SBF, the Young's moduli of HACs are found to degrade with the immersion periods. From the Table 2, a continuous

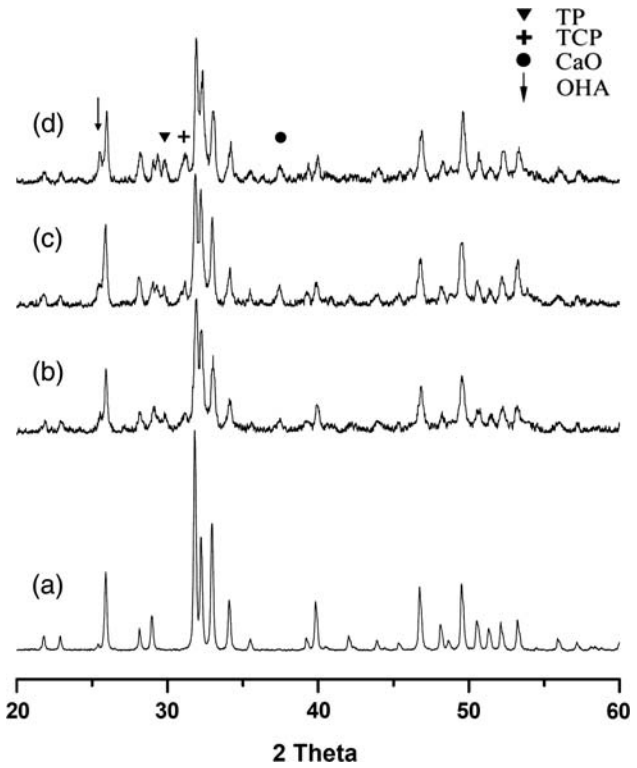

Fig. 6 The diffractograms of the (**a**) HA powder; (**b**) 50 μm-HAC; (**c**) 200 μm HAC and (**d**) subsurface layer of 200 μm HAC

degradation from 22.1 GPa at 1 week to 17.3 GPa at 4 weeks is noted. After 4 weeks of immersion, a total of about 30% reduction in Young's modulus is measured. From the Table 2, we noted that the as-sprayed HAC with the lowest porosity content exhibits a higher Young's modulus than the soaked HACs with higher porosity content, i.e., the porosity in the coating reduces the Young's moduli of the HACs. In the literature [18], the correlation of Young's modulus and the volume fraction of porosity for the sintered alumina have been established.

Bonding strength of HACs

The results of bonding strength, measured by the adhesion test at the HAC/Ti–6Al–4V interface with and without the immersion in SBF are listed in Table 2. For the 200 μm-HAC, the bonding strength of the as-sprayed HAC is 30.2 ± 2.1 MPa which is the highest among the data. After SBF immersion, variation of bonding strength with the immersion time indicates that the bonding strength decays with time to record 19.5 ± 2.7 MPa at 4 weeks of immersion, a total of about 35.4% reduction in bonding strength. For the 50 μm-HAC, the maximum bonding strength measured was 55.4 ± 2.6 MPa (as-sprayed HAC), the measured bonding strength data of the 50 μm HAC, an invalid test, represent to some extent the strength of the glue (~ 60 MPa) that might penetrate to the HAC/Ti interface. The results of this investigation with the thicker coating should apply qualitatively to the thinner HAC on Ti-implants.

Shear strength between bone and HAC

The surgical operations were tolerated well by the dogs, with no complications noted. At harvesting, all implants were clinically stable and no signs of inflammation or adverse tissue reactions could be seen near the implant sites. The interface shear strength data obtained from the push-out tests are summarized in Table 3. The mean value of shear strength for 50 μm thick HAC implants was significantly higher than that of 200 μm thick HAC implants at each time period. The maximum mean shear strength was 14.31 ± 2.73 MPa for the 50 μm-HAC implant at 8 weeks and 10.59 ± 1.05 MPa for the 200 μm-HACimplants at 6 weeks. These findings suggested that the 50 μm-HAC implants were better than the 200 μm-HAC implants for biologic fixation. In addition, at 12 weeks, a slight decrease in mean strength data was found for all implant types.

Failure mode after push-out test

For 50 μm-HAC implants, the failure site was conclusively at or near the HAC–bone interface (Fig. 7). It is clear from Fig. 7a–c that the amount of bone attached to the HAC surface increased with implantation time from 4 to 8 weeks. At 8 weeks, the fractograph was almost covered by bone,

Table 2 Characteristics and mechanical properties of the plasma-sprayed HACs following immersion in SBF

Immersion periods	50 μm HAC			200 μm HAC			1 mm HAC
	IOC (%)	Porosity (%)	Bonding strength (MPa)	IOC (%)	Porosity (%)	Bonding strength (MPa)	Young's modulus (GPa)
As-sprayed	45.5	5.5 ± 0.4	55.4 ± 2.6	47.8	5.2 ± 0.5	30.2 ± 2.1	24.8
1 week	50.3	6.4 ± 0.5	55.2 ± 2.7	52.5	6.3 ± 0.4	26.8 ± 2.4	22.1
2 weeks	57.4	7.9 ± 0.3	53.7 ± 2.8	57.5	7.7 ± 0.5	25.3 ± 3.1	19.4
3 weeks	61.7	8.5 ± 0.4	52.4 ± 3.2	60.3	8.5 ± 0.5	21.7 ± 2.8	18.9
4 weeks	63.4	8.9 ± 0.4	50.8 ± 3.5	62.7	9.1 ± 0.6	19.5 ± 2.7	17.3

Table 3 Results of shear strength (Mean ± SD, MPa) measurements

HAC	4 weeks	6 weeks	8 weeks	12 weeks
50 μm	10.15 ± 1.17	13.14 ± 1.82	14.31 ± 2.73	13.97 ± 3.11
200 μm	8.21 ± 1.06	10.59 ± 1.05	10.24 ± 1.27	9.24 ± 1.61

indicating that the bonding between the bone and HAC might be as strong as the new bone itself, if not stronger. However, at 12 weeks, the amount of bone attached to the HAC surface decreased slightly as compared to that of 8 weeks of post-implantation. The failure modes for 200 μm-HAC implants after different periods of implantation were variable (Fig. 8). It is clear from Fig. 8a that the failure site was at the HAC–bone interface 4 weeks after insertion. At 6 weeks the failure mode was always found inside the HAC lamellar splat layer (Fig. 8b). With an increase in survival time to 8 and 12 weeks, however, a failure at the HAC–Ti alloy substrate interface was observed (Figs. 8c, d).

Residual stresses of HACs

Measurements of $\Delta d/d$ vs. $sin^2\psi$ for the two different HACs (50, 200 μm) acquired by using XRD method are shown in Figs. 9 and 10. After calculation by using Eq. 2, the biaxial state of residual stresses at 0°, 45°, 90° with respect to the spraying direction are shown in Table 4. The residual stresses at 0°, 45°, 90° with respect to the spraying direction (i.e., $\sigma_{0°}$, $\sigma_{45°}$, $\sigma_{90°}$) for the HA coatings were all compressive, and from which the principal stresses (σ_1, σ_2) were calculated. The directions of principal stresses were in proximity to and perpendicular to the spraying direction. In addition, the thicker HAC (200 μm) show the higher residual stress than the thinner HAC (50 μm).

Discussions

It is known that Young's modulus is a function of structural characteristics such as porosity, crystallinity and phase composition, being different for the same material arising from different processing as shown in Table 5. The Young's modulus of 108 GPa for the claimed dense HA was measured with the ultrasonic interferometry technique by Rao et al. [19] without mentioning the porosity content. De With et al. [20] sintered the commercial HA powder to different densities and obtained the corresponding Young's moduli based on the pulsed-echo technique. The Young's modulus of 117 GPa for the fully-dense HA can be deduced from extrapolation of the data to the 0% porosity content. The Young's moduli for the bulk HA by Akao et al. [21] indicated a maximum of 87.8 GPa for the material with 2.8% porosity content sintered at 1,300 °C.

The elastic modulus of the thermally-sprayed coatings is quite different from the bulk materials due to their unique microstructure, inhomogeneity and even post-treatment [22–24]. Tsui et al. [25] deduced the Young's modulus of the plasma-sprayed HAC from conducting the cantilever-beam bending test of the composite specimen containing both HAC and substrate. Han et al. [26] employed the hole-drilling method to measure the residual stress in plasma-sprayed HA, in which an apparently estimated Young's modulus of 81 GPa was used to calculate the residual stress in the coating (Table 5). As shown in Table 5, the Young's modulus of 24.8 GPa for the as-

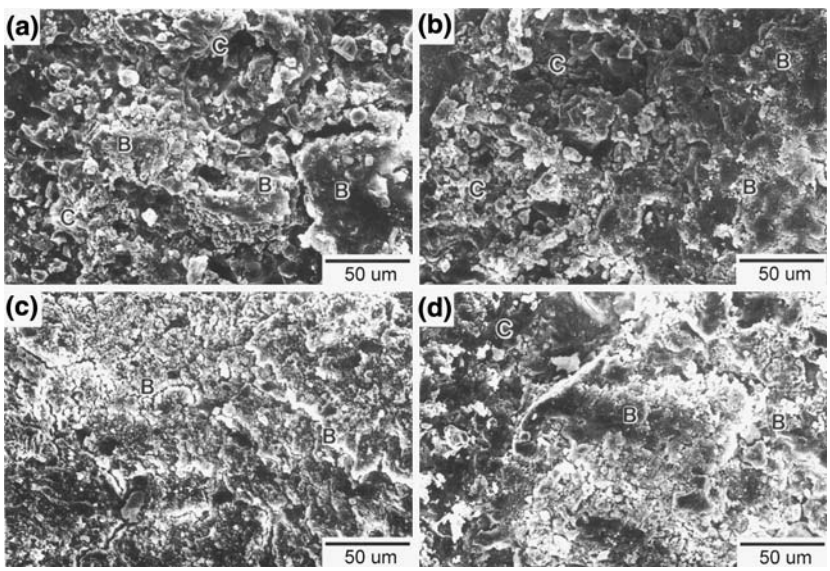

Fig. 7 The SEM fractographs of 50 μm-HAC implants showing that the failure were conclusively at the HAC–bone interface: (**a**) 4 weeks; (**b**) 6 weeks; (**c**) 8 weeks and (**d**) 12 weeks. C, HAC; B, bone

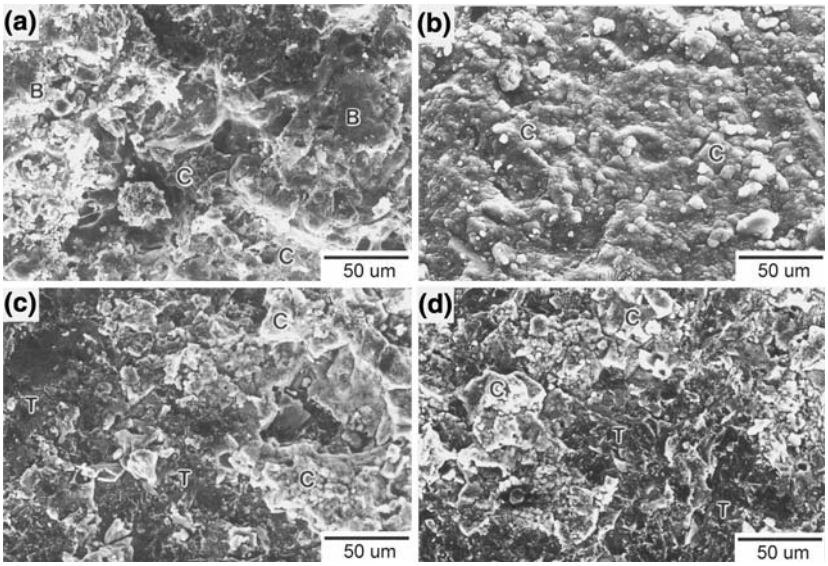

Fig. 8 The SEM fractographs of 200 μm-HAC implants showing failure modes occurred at: (**a**) the HAC–bone interface after 4 weeks, (**b**) inside the coating layer after 6 weeks, (**c**) the HAC–Ti alloy substrate interface after 8 weeks and (**d**) the HAC–Ti alloy substrate interface after12 weeks. C, HAC; B: bone; Ti, Ti alloy

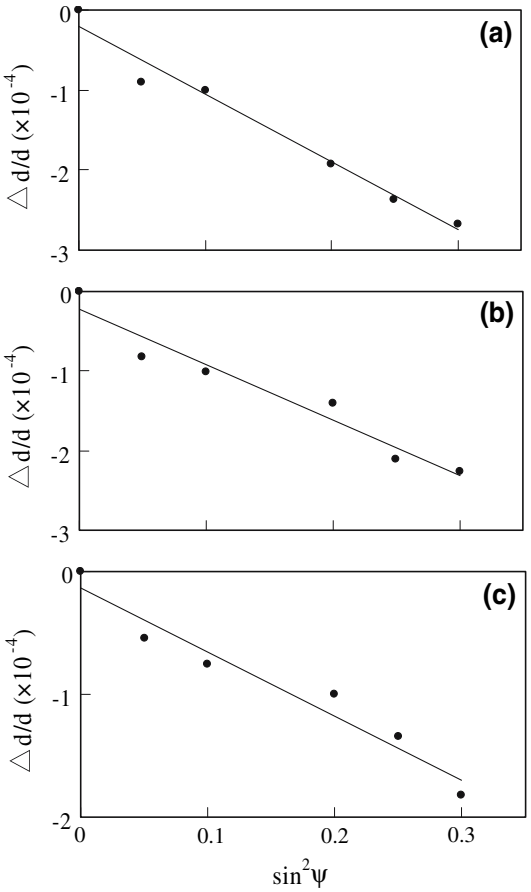

Fig. 9 Δd/d vs. $sin^2\psi$ plot of 50 μm HAC at (**a**) 0°; (**b**) 45°, and (**c**) 90° w.r.t. the spraying direction

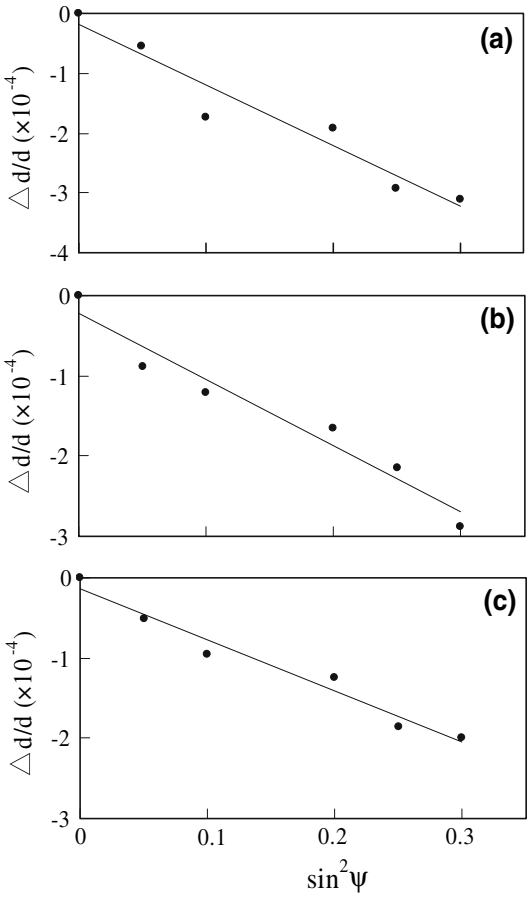

Fig. 10 Δd/d vs. $sin^2\psi$ plot of 200 μm HAC at (**a**) 0°, (**b**) 45°, and (**c**) 90° w.r.t. the spraying direction

sprayed specimen in this study is higher than the previous work (16.2 GPa) [12]. Owing to a better packing effect, the present consolidated HACs contain less porosity with more uniform coating structure than the previous HACs [12]. From the result of immersion in SBF, the Young's moduli of the HACs are found to degrade with the immersion

Table 4 Measured residual stresses (MPa) of HACs; negative value means a compressive stress

HAC	σ_{0°	σ_{45°	σ_{90°	σ_1	σ_2
50 μm	−21.0	−17.3	−13.0	−21.3	−12.8
200 μm	−25.2	−20.5	−15.8	−25.6	−15.5

σ_{0°, stress parallel to the spraying direction; σ_{45°, stress along 45°direction to the spraying direction; σ_{90°, stress perpendicular to the spraying direction; σ_1, major principal stress; σ_2, minor principal stress

Table 5 Young's moduli of hydroxyapatite coatings from various studies

	HA types	Porosity (vol. %)	Young's Modulus (GPa)	
			Method	Value
Bulk HA				
Akao et al.	Sintered at 1,300 °C	2.8	—	87.8
De With et al.	Sintered at 1,250 °C	0	Plused-echo technique	117
Rao et al.	Synthetic HAP compact	Low	Ultrasonic interferometry	108
HA coating				
Tsui et al.	VPS	8.6	Cantilever-beam bending [b]	4.3 [d]
Yang et al.	APS	8.8 [a]	Three-point bending [c]	16.2
Han et al.	APS	—	—	81 [e]
Yang et al. [this study]	APS (as-sprayed)	5.5	Three-point bending [c]	24.8
	APS (4-week immersion)	8.9	Three-point bending [c]	17.3

Negative value of residual stress means a compressive stress. APS, atmosphere plasma spray; VPS, vacuum plasma spray; CDS, high velocity oxyfuel process

[a] Value is the average of 130 data

[b] Composite of HAC and substrate

[c] Free HAC

[d] Average value

[e] Estimated value

periods (Table 2), and a total of about 30% reduction in Young's modulus was obtained after 4 weeks of immersion. The excellent correlation in Table 2 indicates that the porosity in the coating weakens the Young's moduli of the HACs. Sergo et al. [8] also reported that the Young's modulus might be a function of porosity.

For the durability of the system to succeed in application, the residual stress of plasma-sprayed hydroxyapatite coatings on a titanium substrate for orthopaedic use might be very important. In previous work [27], we have evaluated the effect of coating thickness on the bonding strength (coating on titanium substrate) of plasma-sprayed HACs by adhesive test (ASTM C-633). The bonding strength of 200 μm-HAC (27.15 ± 1.75 MPa) was lower than that of 50 μm-HAC (50.21 ± 2.14 MPa), although the validity of bonding strength for thin HAC has been in dispute. In this study, the compressive residual stresses increase with the thickness of coating, therefore, the 200 μm-HAC subjected to high residual tensile stress in the through-thickness direction and lead to the weak bonding strength between coating and substrate. This could be demonstrated that why the 200 μm-HAC revealed the lower bonding strength between the coating and substrate.

During clinical use of hydroxyapatite-coated implant, failures could occur at the coating/substrate interface [28, 29]. In the similar in vivo test, mechanical failure was noted to occur at the same location in the push-out tests [30–32]. One of the reasons that HAC delaminates from the metal implant is the insufficient adhesion between the ceramic material and the substrate [28]. In addition to the HAC degradation, the in-plane compressive stress existed at the implant surface might induce the through-thickness tensile stress that is likely to weaken the adhesion between the HAC and Ti-substrate [6].

An oxide layer in compression on a metallic substrate (semi-infinite plate geometry) will buckle if the compressive stress reaches a critical value: [4]

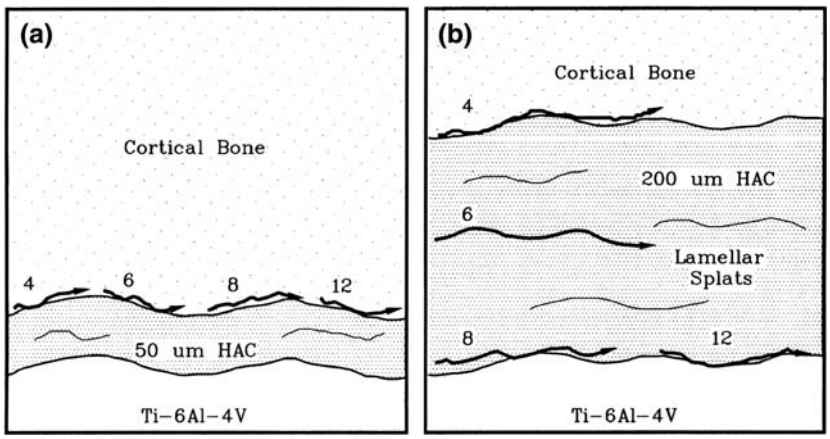

Fig. 11 Schematic representation of failure modes of HAC implants to bone. The 50 μm-HAC implants failed in all case at the HAC–bone interface; however, the 200 μm-HAC implants failed at the HAC–bone interface (4 weeks), inside the HAC layer (6 weeks), and at the HAC–Ti alloy substrate interface (8 and 12 weeks)

$$\sigma_{\text{compress}} \geq \sigma_{\text{buckle}} = \frac{kE_{\text{ox}}}{12(1-v_{\text{ox}}^2)}\left(\frac{t}{c}\right)^2$$

provide a separation (radius c) pre-exists at the oxide/substrate interface (k is a constant $\cong$ 14.7). In the equation E_{ox} and v_{ox} are the Young's modulus and Poisson's ratio of the oxide coating, respectively; and t is the thickness of the oxide coating. Therefore, the pre-existing residual stress or strain in the coating deposited on the stem may be added to the subjected compressive strain in the stem or coating [33], which then affects the coating's performance. It is of interest to understand the mechanical properties and the residual stress and strain states of the hydroxyapatite coatings on the titanium substrate as well as the fracture behavior of the HACs after in vivo test.

In this study, the failure modes of HAC implants to bone after a push-out test are schematically summarized in Fig. 11. From the observation that the 50 μm-HACs neither fractured inside the coating layer nor separated from the substrate up to 12 weeks of post implantation (Fig. 7), it is apparently demonstrated that the 50 μm-HACs with high bonding strength could provide a strong fixation to bone. As the bone progressively apposed with time, the shear strength increased and the maximum shear strength (14.31 ± 2.73 MPa) was reached at 8 weeks of post insertion. At 12 weeks the degradation of HACs or the remodelling of bone might account for the slight decrease in the shear strength. From the Fig. 11b, the failure modes occurred either inside the coating lamellar splat layer (Fig. 8b) or at the HAC–Ti interface (Fig. 8c, d), which indicated that the 200 μm-HACs with weak bonding strength could not provide reliable fixation to bone.

As a consequence, the results of shear strength measurements for both implants might be influenced by the apposition of bone, the residual stress in the HAC, and its degradation in body fluid. From our previous work [7], the HAC structure was degraded and its cohesive strength decreased severely after the attack of the simulated body fluid. However, in the case of this study, there was no difference in the physiological environment and the structures for 50 and 200 μm-HAC were the same, meaning the same coating degradation and similar cohesive strength in both HA coatings. Meanwhile, the apposition of bone to 50 and 200 μm-HACs should not make a difference. Hence, the difference in shear strength could best attributed to the compressive residual stress in the coating. It is concluded that the compressive residual stress of 200 μm-HAC is higher than 50 μm-HAC, therefore, it subjected to high residual tensile stress in the through-thickness direction and lead to the weak bonding strength between the lamellar splat layer and in the HAC–Ti interface. Besides, HAC would be degrading with time under the attack of body fluid. That is why as the apposition of bone increased with the implantation time, the fracture side of 200 μm-HAC was moved toward to the HAC–Ti interface.

With regard to the biological implication of residual stress in the plasma-sprayed HAC, Otani et al. [33] obtained the strain distribution of 0.091–0.084% in the proximal femur with Ti6Al4V component under 2,000 N axial loads. The pre-existing residual compressive stress in HAC evaluated in the present work are of comparable or larger magnitude than the loading strain on the HAC as inferred from the study of Otani et al. Therefore, the residual strain existed in the HAC might be a significant factor for the durability of the coating on an artificial implant as implied by Eq. 3. Residual stress in the compressive state of plasma-sprayed ceramic coatings on metal substrate tends to delaminate the coatings from the substrate per Eq. 3 [4]. The stress is reasonably suspected to act adversely on the bonding strength in vitro test and the shear strength in vivo test of the HA coated titanium implants.

Conclusions

The effects of residual stress in the various coating thickness, namely 50 and 200 μm, on the in vivo shear strength and failure mode of plasma-sprayed HAC implant in the

femora of canines were studied. The concluding remarks of this study are summarized as follows: (1) Results of the push-out tests showed that the shear strength of 50 μm-HAC implants was significantly higher than that of 200 μm-HAC implants at all time periods. (2) The failure mode for 50 μm-HACs was in all cases at the HAC–bone interface. (3) For 200 μm-HAC, failure was found at the HAC–bone interface, inside the lamellar splat layer, and at the HAC–Ti alloy substrate interface, after 4, 6, and 8–12 weeks of insertion, respectively. (4) The variation of the failure mode of 200 μm-HAC with time could not be accounted for by the attack of body fluid alone. The degradation must be caused mainly by the compressive residual stress in the coting. (5) Significantly, the thicker 200 μm-HA coating exhibited higher residual stress and poor mechanical stability in vivo, as compared with the thinner 50 μm-HA coating having lower residual stress and superior performance. These results supported our assertion of the importance of residual stress in plasma-sprayed hydroxyapatite coatings.

References

1. S. PAOLO, L. MATTEO and B. LUCA, *Thin Solid Films* **278** (1996) 96
2. S. KURODA and T. W. CLYNE, *Thin solid films.* **200** (1991) 49
3. S. TAKEUCHI, M. ITO and K. TAKEDA, *Surf. Coat. Technol.* **43/44** (1990) 426
4. A. G. EVANS, G. B. CRUMLEY and R. F. DEMARAY, *Oxid. Met.* **20** (1983) 196
5. R. MEVREL, *Mater. Sci. Technol.* **3** (1987) 531
6. Y. C. YANG and E. CHANG, *Biomaterials.* **22** (2001) 1827
7. Y. C. YANG, E. CHANG and S. Y. LEE, *J. Biomed. Mater. Res.* **67A** (2003) 886
8. V. SERGO, O. SBAIZERO and R. D. CLARKE, *Biomaterials.* **18** (1997) 477
9. R. G. GEESINK, K. de GROOT and C. P. KLEIN, *Clin. Orthop.* **225** (1987) 147
10. S. D. COOK, K. A. THOMAS, J. F. KAY and M. JARCHO, *Clin. Orthop.* **232** (1988) 225
11. K. SOBALLE, E. S. HANSEN, H. B. RASMUSSEN, C. M. PEDERSEN and C. BUNGER, *Acta. Orthop. Scand.* **61** (1990) 299
12. Y. C. YANG, E. CHANG, B. H. HWANG and S. Y. LEE, *Biomaterials.* **21** (2000) 1327
13. T. KOKUBO, In CRC handbook of bioactive ceramics vol. 1. T. Yamamuro, L. L. Hench, J. Wilson (eds). (CRC Press, Florida 1990) p. 41
14. ASTM E855-90. Standard test methods for bend testing of metallic flat materials for spring applications involving static loading. American Society for Testing Materials (1990)
15. ASTM C 633-79. Standard test method for adhesion or cohesive strength of flame-sprayed coatings
16. K. de GROOT, C. P. A. T. KLEIN, J. G. C. WOLKE and J. M. A. de BLIECK-HOGER-VORST, in CRC Handbook of Bioactive Ceramics vol. II. edited by T. Yamamuro, L. L. Hench, J. Wilson (CRC Press Inc., Boca Raton, Florida, 1990) pp. 133–142
17. K. A. GROSS and C. C. BERNDT, *J. Mater. Sci. Mater. Med.* **5** (1994) 219
18. R. L. COBLE and W. D. KINGERY, *J. Am. Ceram. Soc.* **39[11]** (1956) 381
19. H. RAO, W. A. THOMPSON, J. L. KATZ and R. A. HARPER, *J. Dent. Res.* **55** (1976) 708
20. G. de WITH, H. J. A. VANDIJK, N. HATTU and K. PRIJS, *J. Mater. Sci.* **16** (1981) 1592
21. M. AKAO, H. AOKI and K. KATO, *J. Mater. Sci.* **16** (1981) 809
22. H. E. EATON and R. C. NOVAK, *Surf. Coat. Technol.* **27** (1986) 257
23. C. J. LI, A. OHMORI and R. MCPHERSON, *J. Mater. Sci.* **32** (1997) 997
24. K. S. SHI, Z. Y. QIAN and M. S. ZHUANG, *J. Am. Ceram. Soc.* **71** (1998) 924
25. Y. C. TSUI, C. DOYLE and T. W. CLYNE, *Biomaterials* **19** (1998) 2015
26. Y. HAN, K. W. XU and J. LU, *J. Biomed. Mater. Res.* **26** (2001) 596
27. B. C. WANG, E. CHANG, C. Y. YANG, D. TU and C. H. TSAI, *Surf. Coat. Technol.* **58** (1993) 107
28. W. THOMAS, C. T. RUDOLPH, Z. RICHARD and T. JAMES, *J. Bone. Joint Surg. (American volume)* **73A** (1991) 1452
29. W.P. HU, K. A. LAI, C. H. LIN, C. Y. YANG and G. L. CHANG, in Bioengineering, Proceedings of the Northeast Conference IEEE 28th Annual Northeast Bioengineering Conference Apr 20–21 2002
30. J. M. SPIVAK, J. L. RICCI, N. C. BLUMENTHAL and H. ALEXANDER, *J. Biomed. Mater. Res.* **24** (1990) 1121
31. K. HAYASHI, T. MASHIMA and K. UENOYAMA, *Biomaterials.* **20** (1999) 111
32. T. INADOME, K. HAYASHI, Y. NAKASHIMA, H. TSUMURA and Y. SUGIOKA, *J. Biomed. Mater. Res.* **29** (1995) 19
33. T. OTANI, L. A. WHITESIDE and S. E. WHITE, *J. Biomed. Mater. Res.* **27** (1993) 575